Sensors & Actuators: B. Chemical 282 (2019) 567–573

Contents lists available at ScienceDirect

Sensors and Actuators B: Chemical

journal homepage: www.elsevier.com/locate/snb

Ppb-level photoacoustic sensor system for saturation-free CO detection of SF_6 decomposition by use of a 10 W fiber-amplified near-infrared diode laser

Xukun Yin[a,b,c,1], Hongpeng Wu[a,b,1], Lei Dong[a,b,*], Weiguang Ma[a,b], Lei Zhang[a,b], Wangbao Yin[a,b], Liantuan Xiao[a,b], Suotang Jia[a,b], Frank K. Tittel[c]

[a] State Key Laboratory of Quantum Optics and Quantum Optics Devices, Institute of Laser Spectroscopy, Shanxi University, Taiyuan, 030006, China
[b] Collaborative Innovation Center of Extreme Optics, Shanxi University, Taiyuan, 030006, China
[c] Department of Electrical and Computer Engineering, Rice University, Houston, TX, 77005, USA

ARTICLE INFO

Keywords:
Photoacoustic spectroscopy
Trace gas sensor
Sulphur hexafluoride
Erbium doped fiber amplifier
Differential photoacoustic cell

ABSTRACT

A photoacoustic sensor system for the ppb-level CO detection of sulphur hexafluoride (SF_6) decomposition was developed by use of a 10 W fiber-amplified near-infrared (NIR) diode laser. A photoacoustic detection module with symmetrical construction was designed to allow a high power laser beam and a large gas flow. A theoretical model was developed to describe the dynamic equilibrium processes of CO molecular activation and deactivation in the presence of gas flow. The 10 W optical excitation power effectively compensates the CO weak absorption line strength in the NIR spectral region and realizes a saturation-free CO detection with the assistance of the gas flow, resulting in a ppb-level CO detection sensitivity, which is comparable with the detection sensitivity obtained using a mid-infrared CO sensor.

1. Introduction

Sulphur hexafluoride (SF_6) has been selected as the industry's preferred gas for electrical insulation, current interruption and arc quenching in electric power transmission and distribution of electricity, due to its thermal and chemical inertness, dielectric properties, nonflammability and nontoxicity. However, SF_6 can be decomposed into lower fluorides of sulphur (SF_2, SF_3 and SF_4) by three fundamental processes: electronic, thermal and optical in the presence of an electric arc, spark, partial corona discharge as well as superheating in high voltage gas-insulated equipment [1,2]. The generated sulphur fluorides will react with gas impurities and electrodes to form numerous chemically active gaseous by-products (such as CO, SO_2, H_2S, CF_4 and SOF_2) and solid by-products (fluoride powder). Although the gaseous by-products have little effect on the insulation strength, the presence and accumulation of these corrosive gases can lead to a chemical attack of solid insulating materials, posing a possible threat to personnel safety and equipment compatibility problems. Furthermore, the decomposition rates and ratios of SF_6, and compositions of these gaseous by-products depend on the specific partial discharge insulating defect. Therefore, it is necessary to establish a relationship between the SF_6 decompositions and the internal condition of the gas-insulated equipment in order to determine and confirm the causes and the fault types [3–6]. Early detection of SF_6 decompositions can provide a crucial way to predict and avoid fatal failure. The ability to detect trace gaseous CO in SF_6 is of interest because of recent measurements and calculations which shows that CO can be produced during insulation aging and other organic material decomposition reactions [7]. Therefore, it is desirable to develop a compact, robust, cost-effective, highly reliable and sensitive CO gas sensor with a minimum detection limit of < 1 ppm for SF_6 decomposition detection in electric power systems.

Up to now, various trace gas sensors for the detection of SF_6 decomposition have been reported, such as gas chromatography [4], ion mobility spectrometers [5], detector nanotubes [6] and electrochemical sensors [8]. However, most of these sensors have a long response time and a short service life. Additionally, none of them is appropriate to be used for online detection. Recently, laser-based absorption spectroscopy for trace gas detection has been rapidly developed, which offers the advantage of a faster response time (< 1 s), higher detection selectivity and sensitivity as well as real time *in-situ* measurements [9–14]. In 2015, four characteristic gases (SOF_2, SO_2F_2, SO_2 and CO) were measured by a Fourier transform infrared spectroscopy (FTIR) spectrometer but without a quantitative analysis [15]. The same year, a non-resonant photoacoustic spectroscopy (PAS) sensor was developed to

* Corresponding author at: State Key Laboratory of Quantum Optics and Quantum Optics Devices, Institute of Laser Spectroscopy, Shanxi University, Taiyuan, 030006, China.
E-mail address: donglei@sxu.edu.cn (L. Dong).
[1] These authors contributed equally to the manuscript

https://doi.org/10.1016/j.snb.2018.11.100
Received 6 August 2018; Received in revised form 18 November 2018; Accepted 19 November 2018
Available online 22 November 2018

continuously detect CO, SO_2 and CF_4 with detection limits of 5.9, 8.3 and 5.5 ppm, respectively [16]. In 2016, a cantilever enhanced photoacoustic spectrometry (CEPAS) platform was used to detect H_2S in a SF_6 buffer gas and a detection limit of 1.75 ppm was obtained [17]. In 2017, a novel photoacoustic cell was used to detect trace H_2S and SO_2 and after optimization the minimum detection limit of 109 ppb and 74 ppb was achieved with an averaging time of 1 s [18,19]. These sensors were functional in a particular application, but none of them could meet the actual CO detection sensitivity requirement of < 1 ppm in a SF_6 decomposition analysis. Hence, there is a strong demand to develop a new CO gas sensor capable of operating in a SF_6 buffer gas environment to predict and avoid the potential risk in electric power systems.

Numerous optical trace CO sensors based on PAS in N_2 or air buffer gases have been demonstrated mostly in the spectral region from 1 to 5 μm, which covers the fundamental, the first and the second overtone absorption bands of CO. The fundamental ro-vibration band is actually the strongest infrared absorption band of CO and a detection sensitivity down to the ppb-level was achieved due to the strong absorption coefficient [20–22]. However, SF_6 possesses continuous unidentified absorption spectra between 3.3 μm and 10 μm, and therefore it is not possible to detect SF_6 decompositions in this spectral region [15,19]. One of the significant advantages of PAS technique is that its sensitivity is directly proportional to the optical excitation power, which implies that the sensor's performance can be improved with increased laser excitation power. Although the absorption line intensity in the near-infrared (NIR) spectral region is lower by 2–4 orders of magnitude than that in the mid-infrared (MIR) region, NIR telecommunication diode lasers can be attractive, since they can be easily operated at room temperature with a long service life and low cost. Furthermore their output power can be readily boosted up to the watt level or even higher by use of commercially available optical fiber amplifier systems [23–26].

High output power of the optical excitation source can compensate the sensitivity loss of low absorption line intensity, but some inevitable problems may appear in practical applications when the laser power increases to the watt level, such as a degraded beam quality, severe window noise, difficult optical alignment and potential saturation effects. Some measures have to be taken in order to address these issues. In this paper, a ppb-level CO sensor system was developed, satisfying the detection requirement of SF_6 decomposition in electric power systems. A NIR telecommunication diode laser with an amplified optical power of 10 W was employed to compensate the CO weak absorption line strength in the NIR spectral region and thereby obtain a comparable detection limit as in the MIR spectral region. A twin-channel differential photoacoustic cell (DPAC) was designed to resolve the above mentioned issues in the case of high optical excitation power. The detection sensitivity of the CO sensor system was investigated and optimized in terms of gas concentration, flow, pressure and activation-deactivation processes of CO molecules at high optical excitation power levels.

2. Selection of detection wavelength and optical excitation source

The SF_6 concentration in an electric power system is usually > 99.8%, which means that the detection of the trace gaseous decomposition is operated in a pure SF_6 buffer gas rather than in N_2 or air environment as usual. Several SF_6 physical constants such as the density, thermal conductivity, molar mass, specific heat and viscosity strongly differ from those applicable to N_2 or air. Moreover, the SF_6 molecule has been proven to have an absorption spectrum in the MIR spectral range, which may result in the unwanted signal interference between the SF_6 and its decomposition for PAS [19]. According to the *HITRAN* database [27], SF_6 absorption lines were calculated based upon the global effective Hamiltonian (EH) parameters, which includes the strong ν_3 band and the hot band (ν_4 and $\nu_4+\nu_6-\nu_6$). However, the absorption line listed in the *HITRAN* database just covers the spectral range from 10 to 17.2 μm [28]. Some unresolved SF_6 absorbance spectra were experimentally observed between 3.3 μm and 10 μm by a FTIR spectrometer (Thermofisher Nicolet IS50) when pure SF_6 gas (> 99.99%) was analyzed, as shown in Fig. 1. The FTIR spectrometer was equipped with a multipass gas cell of 9.5 m path length, which allows the detection of the weak SF_6 and CO absorption spectra within the wavelength range of < 5 μm A flat and clear spectral region between 1 μm and 3.3 μm was obtained, which is an ideal region for SF_6 composition detection.

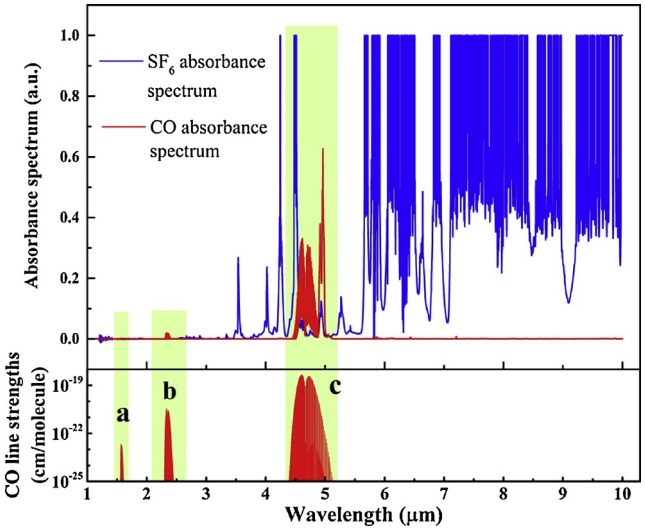

Fig. 1. Upper part: continuous pure SF_6 [19] and 0.1% CO/N_2 gas mixture absorbance spectrum curves obtained by the FTIR spectrometer between 1 μm–10 μm; Bottom part: three main CO absorption bands falling in the infrared region according to the *HITRAN* database.

As shown in the bottom part of Fig. 1, the CO molecule has three main absorption bands in the infrared spectral region: a. the second overtone band located near 1.56 μm, b. the first overtone band located around 2.33 μm and c. the fundamental band located around 4.7 μm. For a comparison, a 0.1% CO/N_2 gas mixture was introduced into the multipass gas cell. Continuous spectral scanning was carried out by the FTIR spectrometer between 1 μm–10 μm, as depicted in the upper part of Fig. 1. An unfamiliar absorption peak located at around 4.8 μm is due to iron-pentacarbonyl ($Fe(CO)_5$), which was formed by CO and the steel cylinder at high pressures and which can be avoided by using an aluminum cylinder. Hence the fundamental band (4.7 μm) of CO was not used to quantify the CO concentration since cross-talking occurs between the spectra of CO and SF_6.

In the NIR spectral region, the absorption line intensity in the first overtone band (2.33 μm) is stronger by two orders of magnitude than in the second overtone band (1.56 μm). However, the output power of commercially available lasers is at a few mW-level, which limits the gas detection performance. Although the second overtone band (1.56 μm) possesses the lowest absorption line strength in the three absorption bands, it is located at the wavelength window for optical fiber communication. Optical fiber communication equipment, such as an optical fiber amplifier can be employed to provide significant optical signal amplification. The boosted optical power is higher by 3–4 orders of magnitude than the available optical power in the fundamental and the first overtone bands and thereby readily compensates the weak absorption line strength in the second overtone band by means of the PAS technique. In our sensor system, a continuous-wave fiber-coupled distributed feedback (CW-DFB) laser with a center wave-length of 1566.3 nm (Sichuan Tengguang Electronics and Technology Co., China, Model 914010C) was chosen as the optical excitation source and a two-stage erbium-doped fiber amplifier (EDFA) with an output power of 10 W was employed to enhance the diode laser output power.

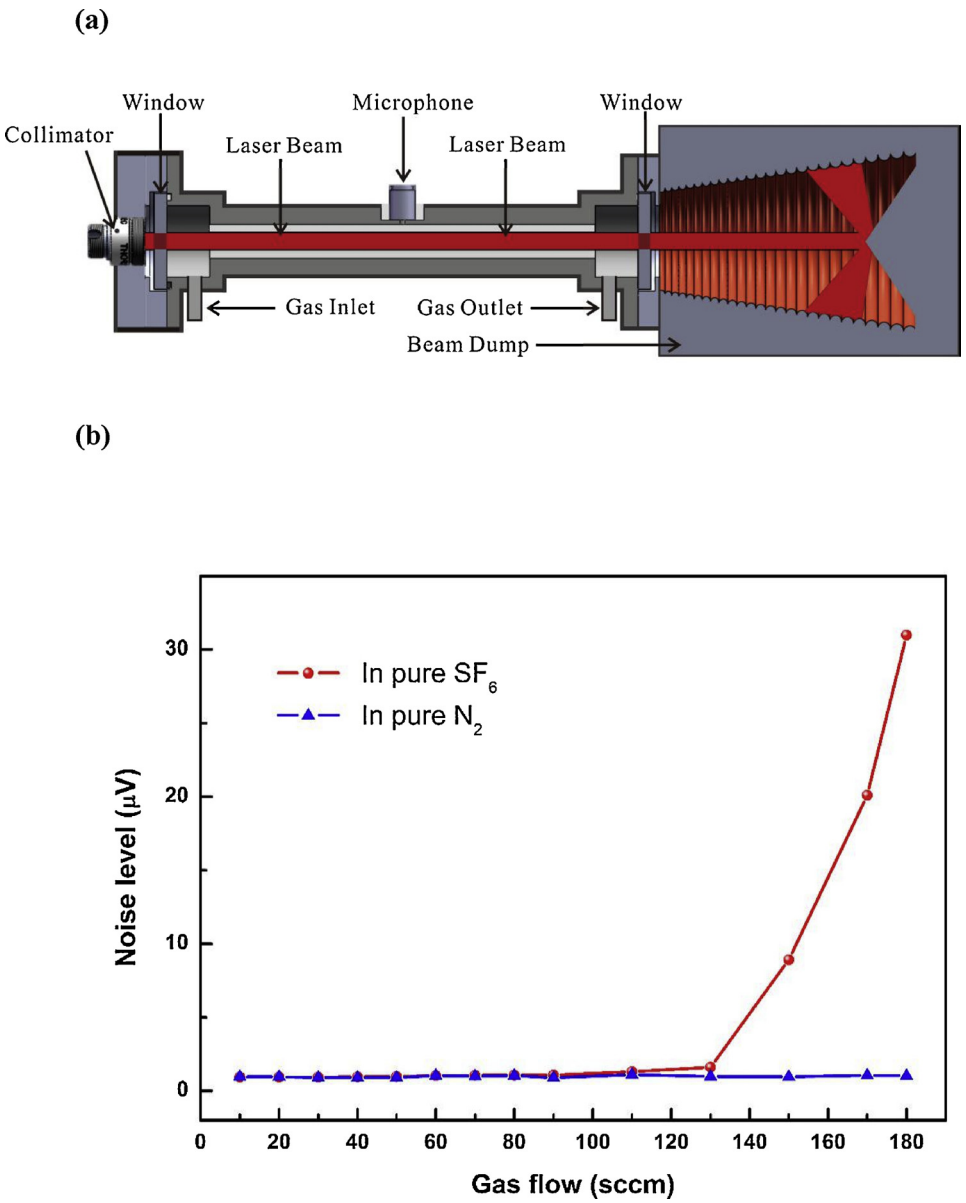

Fig. 2. (a) Schematic of low gas flow noise photoacoustic detection module for the high power laser beam; (**b**) Gas flow noise as a function of the gas flow.

3. Photoacoustic sensor system

3.1. Design of a photoacoustic detection module

In order to better match the high power diode laser beam, a photoacoustic detection module (PADM) was designed as shown in Fig. 2(a), which includes a DPAC, an embedded optical collimator (Thorlabs, USA, Model F230FC-1550) and a custom reflected-light beam dump. The DPAC has two identical parallel tube-shaped channels with a length of 90 mm and a diameter of 8 mm, which has the same two tube structure with the DPAC as described in Ref [29]. Two buffer volumes (Φ20 × 10 mm) connect to the two channels at both ends, thus making the two channels act as acoustic open-open resonators. The buffer volumes are sealed by two CaF_2 windows coated with highly anti-reflecting films, which effectively decrease the light absorption of the CaF_2 windows and thus reduces window noise. The diameter of the windows is 25.4 mm. Two selected electret condenser cylindrical microphones are installed in the middle of each resonator, having the same frequency response sensitivities. The current signals from these two microphones are directed to a custom transimpedance differential preamplifier to convert the current signal into a voltage signal. The symmetrical resonator construction and differential signal output are used to suppress the noise from the gas flow. The gas flow noise as a function of the gas flows is shown in Fig. 2(b). The results show that the noise levels remain constant with a SF_6 gas flow of < 130 sccm or a N_2 gas flow of < 180 sccm. In fact, the noise level shows no significant variation when the gas flow rate is < 1200 sccm in N_2 buffer gas for the developed PADM. The higher flow noise measured for SF_6 gas is due to its five times heavier molecular weight with respect to N_2 or air. In order to reduce the difficulty and complexity of light path alignment, an optical collimator is mechanically embedded into the photoacoustic cell, in front of the entrance window. The output beam is in line with the cylindrical centerline of one of two resonators. A beam dump is placed behind the output window to collect and absorb the reflected high power light, as shown in Fig. 2(a).

3.2. Setup of photoacoustic sensor system

A schematic of the PAS-based SF_6 decomposition sensor system consisting of the PADM, a CW-DFB laser and an EDFA is depicted in

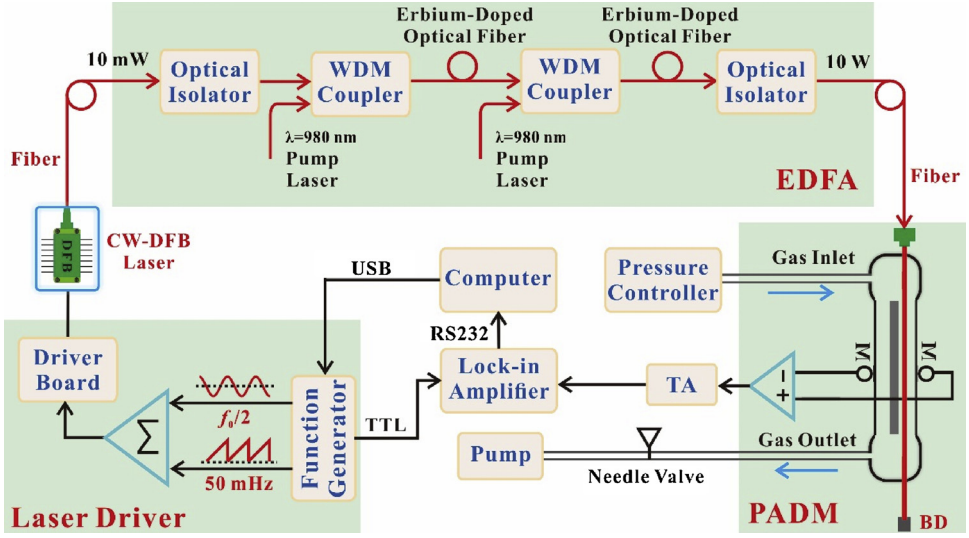

Fig. 3. Schematic of the PAS-based CO sensor system for the SF_6 decomposition analysis based on a differential photoacoustic cell and a 10 W fiber amplifier. EDFA: erbium-doped fiber amplifier; PADM: photoacoustic detection module; BD: beam dump.

Fig. 3. A computer-controlled digital function generator was employed to generate a sinusoidal dither and a 50 mHz ramp signal. The ramp frequency was used to slowly change the laser wavenumber from 6383.3 cm^{-1} to 6382.9 cm^{-1}. In order to realize 2*f* wavelength modulation spectroscopy, the modulation frequency of the sinusoidal wave was set to one half of the DPAC resonance frequency ($f = f_0/2$). The two generated signals were superposed by an electronic adder and then sent to a laser driver board (Wavelength Electronics, USA, Model LDTC0520) to control the laser current. The laser temperature was maintained at 22.0 deg C. The laser beam with an output power of 10 mW was directed to the L-band EDFA with a two-stage amplifier. When the modulated laser beam passed through the Erbium-doped optical fiber, two pump lasers provided the amplified energy at the Erbium absorption peaks of 980 nm, by using wavelength division multiplex (WDM) couplers. Two optical isolators (Connect Laser Technology Ltd., China, Model A12104132) were inserted upstream and downstream to remove residual traces of the pump beam in order to minimize back reflections and interferences with the reception of the signal. The EDFA output power can be varied from 30 mW to 10 W without changing the laser wavelength. The output laser from the EDFA was collimated by an optical fiber collimator with a $1/e^2$ beam diameter of 0.9 mm. A standard TEM_{00} Gaussian laser beam was obtained without the out-of-band light, which allowed the laser beam to pass easily through the 8 mm diameter photoacoustic resonator without touching any surfaces. The excited photoacoustic signal was detected with the embedded microphone and amplified by a transimpedance amplifier with a gain factor of 13. Then the amplified signal was directed to a lock-in amplifier (Stanford Research Systems, USA, Model SR830) to demodulate the photoacoustic signal in the 2*f* mode. A TTL synchronous signal from the function generator was fed into the lock-in amplifier as the reference input. The modulation signal was controlled by the function generator and the data acquired by the sensor system were processed by a computer running in a LabVIEW routine.

CO/SF_6 gas mixtures with different concentration levels between 0–500 ppm were produced by a gas dilution system (Environics Inc., USA, Model EN 4000). A pressure controller (MKS Instrument, USA, Model 649B) was placed upstream to control and maintain the sensor system pressure. A needle valve and a diaphragm pump (KNF Technology Co., Germany, Model N813.5) were placed downstream to control the gas flow rate. All the sensor experiments were operated at room temperature.

3.3. Frequency response of photoacoustic cell

With the resonant DPAC, the modulation frequency of laser wavelength must be tuned to one of the eigenresonances so that the standing waves can form in the resonator. Therefore, it is critical to measure accurately the cell frequency response, determining the resonant frequencies of the cell [30]. The CW-DFB laser wavelength was set at the peak of the CO target line and the EDFA output power was adjusted to 10 W A 500 ppm CO/SF_6 gas mixture was fed into the gas sensor system. At atmospheric pressure and room temperature, the laser modulation frequency was slowly varied in steps of 0.1 Hz in order to obtain the DPAC response curves as shown in Fig. 4. The fundamental (001) and first (002) longitudinal vibrational frequencies of the designed DPAC were found to be $f_{001} = 2f_1 = 690.6$ Hz and $f_{002} = 2f_2 = 2055.2$ Hz, respectively, according to the measured signal amplitudes. The fundamental longitudinal mode was chosen for the following experiment.

4. Relationship between signal amplitude, flow rate and concentration

In the case of high optical excitation power the saturation effect has to be considered in which the signal amplitude depends not only on the gas concentration, but also on the gas flow rate. In order to study the activation-deactivation processes of CO molecules in the infrared

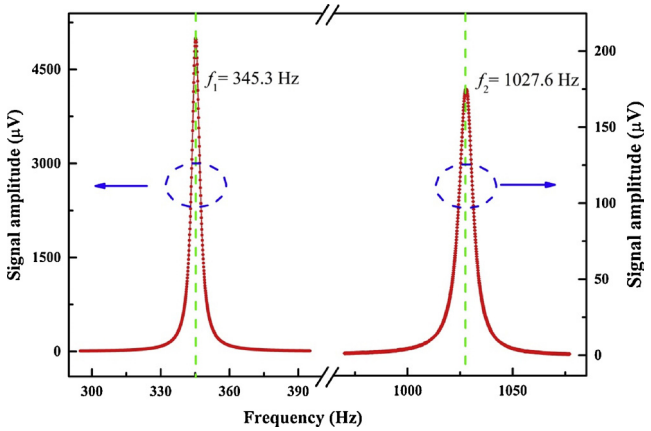

Fig. 4. The fundamental and first longitudinal vibrational signal response curve of the DPAC as a function of frequencies.

spectral region, a simplified two-level model of the absorption process was used to describe the photoacoustic production due to photon absorption. Photons absorbed by molecules result in molecular energy level transitions, such as rotational, vibrational and electronic transitions. Molecules in the excited state lose their energy by radiation processes (spontaneous, stimulated emission and/or collisional relaxation), in which the energy is transformed into translational energy. Thus, the photoacoustic and thermal waves are generated due to localized transient heating and expansion.

We assume that the gas mixture contains target molecules, which can resonantly absorb photons from the illuminating optics source. The concentration of these molecules in the ground state and excited state are represented by N_1 and N_2, respectively. The sum N of ground state and excited state molecules is constant in the quasi-steady state. The absorption of photons is governed by the rate equation of:

$$\frac{dN_2}{dt} + (2k_{st} + k_{sp} + k_r)N_2 = k_{st}N \tag{1}$$

where k_{st} is the rate constant of the stimulated absorption and emission, k_{sp} represents the rate constants of spontaneous emission and k_r denotes the effect of all relaxation processes. The rate constant k_{st} is proportional to the absorption cross section of the excited molecular transition σ and with the photon flux Φ. It can be expressed as:

$$k_{st} = \sigma\Phi = \sigma I/h\nu \tag{2}$$

where I is the excitation light intensity, $h\nu$ represents the energy of the absorbed photons between the excited state and the ground state.

In the case of a low optical excitation power (small photon flux Φ) in the NIR or MIR spectral range, the rate constant k_{st} and k_{sp} are less than the rate constants (k_r). Therefore, with 2f based wavelength modulation (WM), the photoacoustic signal S_{WM} is linearly proportional to the incident optical power P_i, the concentration of the absorbing molecule C and the absorption cross section of the absorbing molecule σ, (*i.e.*, $S_{WM} \propto P_i \times C \times \sigma$) [31]. However, with a strong optical excitation power (strong photon flux Φ), a saturation effect may occur, which implies that the depletion from the vibrational excited level slows with respect to the pump rate and molecules are unable to be excited to higher energy levels. In this case, reloading of 'fresh' ground state molecules should be considered in order to improve the saturated photoacoustic signal. The rate constant of the stimulated absorption-emission k_{st} is considerably greater than the other rate constants (k_{sp} and k_r). Eq. (1) is simplified as:

$$\frac{dN_2}{dt} + 2k_{st}N_2 = k_{st}N \tag{3}$$

In case of the 2f based WM technique, the laser wavelength can be modulated by the laser current. The absorption cross section σ changes with wavelength and is a function of the wavelength λ. Thus, the photoacoustic signal is modulated by modulating the laser current. We assume that the laser center wavelength remains at the peak of a target absorption line and the laser wavelength dither is far less than the line width of the target absorption line. Therefore the absorption cross section $\sigma(\lambda)$ can be replaced with a constant σ_0, which is the absorption cross section at the peak of the target absorption line. Thus, the solution of Eq. (3) can be calculated as:

$$N_2 = \frac{N}{2}\left(1 - e^{-\frac{2\sigma_0 I}{h\nu}t}\right) \tag{4}$$

With increasing time, the saturation effect dominates and the concentration of the excited state molecules N_2 is almost half of all molecules N in the DPAC. Consequently, the photoacoustic signal will not benefit from further higher optical excitation power due to the deficiency of 'fresh' ground state molecules [32–34].

In order to increase the photoacoustic signal amplitude in the case of high optical excitation power, more ground state molecules should be supplemented into the DPAC and thus a part of the supplemented 'fresh' molecules will be excited constantly to the excited state with strong optical excitation power. A qualitative theoretical model was proposed to describe the dynamic equilibrium processes. Considering the gas flow, the rate equation can be represented as:

$$\frac{dN_1}{dt} + k_{st}N_1 = k_{st}N_2 + \frac{R}{V}N_1 \tag{5}$$

where R is the gas flow rate, V is the volume of DPAC. Substituting the equation of $N = N_1 + N_2$, the concentration N_1 in the ground state can be eliminated:

$$\frac{dN_2}{dt} + \left(2k_{st} - \frac{R}{V}\right)N_2 = \left(k_{st} - \frac{R}{V}\right)N \tag{6}$$

The concentration of the excited state molecules N_2 can be written as:

$$N_2 = N\left(1 - \frac{\frac{\sigma_0 I}{h\nu}}{2\frac{\sigma_0 I}{h\nu} - \frac{R}{V}}\right)\left[1 - e^{-\left(2\frac{\sigma_0 I}{h\nu} - \frac{R}{V}\right)t}\right] \tag{7}$$

With increasing time, the concentration of the excited state molecules N_2 can be expressed as:

$$N_2 = N\left(1 - \frac{\frac{\sigma_0 I}{h\nu}}{2\frac{\sigma_0 I}{h\nu} - \frac{R}{V}}\right) < \frac{1}{2}N \tag{8}$$

The excited state molecules N_2 remain less than half of all the molecules N in the DPAC in the presence of the gas flow (R/V). Therefore, a large gas flow supply can effectively minimize the saturation effect. Moreover, a large gas flow rate is advantageous to reduce the gas-exchange time, thereby improving the response time. However, the noise level of the photoacoustic sensor system may increase sharply with an increase of gas flow, especially for a SF_6 buffer gas, which has a 5 times heavier molecular weight than N_2 or air [19]. In our photoacoustic cell design, a symmetrical resonator construction and differential signal output were employed to suppress the gas flow noise as described in Section 3.1.

The following experiment was implemented to verify the theoretical model established above. Three different concentration levels of CO/SF_6 gas mixtures, 100 ppm, 300 ppm and 500 ppm, were fed into the DPAC sequentially. The amplitudes of the 2f photoacoustic signals were recorded as a function of the gas flow rates as shown in Fig. 5. With an increasing gas flow rate, the signal amplitude continuously increased for the three different concentration CO levels. The ground state molecules were complemented and the saturation effect was reduced. When the gas flow of the CO/SF_6 gas mixture is > 18 sccm, the signal amplitude of CO remains constant. This implies that enough ground

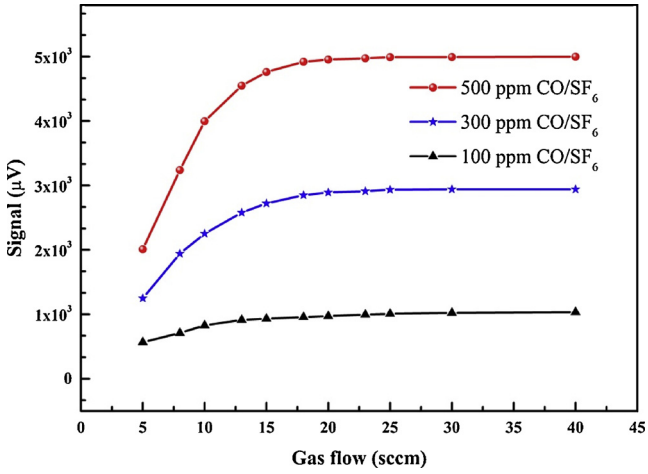

Fig. 5. Dependence of the saturated signal amplitude on the gas flow rate and the gas concentration.

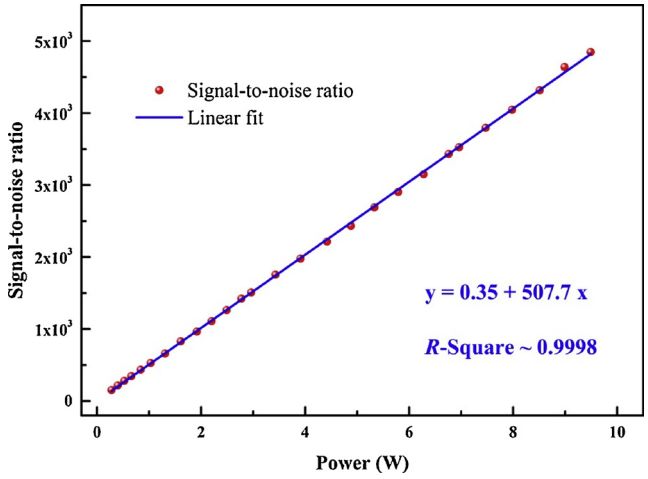

Fig. 6. Power-boosted PAS signal-to-noise ratio as a function of the actual powers measured range from 30 mW to 9.5 W.

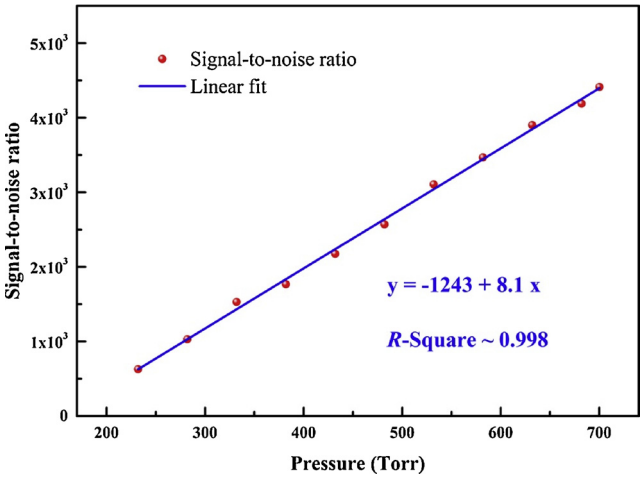

Fig. 7. Relationship between the signal amplitude of a 500 ppm CO/SF_6 gas mixture and the gas pressure inside the differential photoacoustic cell in the range of 230 Torr to 700 Torr.

state molecules are reloaded and the saturation effect is completely eliminated. With the 100 ppm CO/SF_6 gas mixture, the signal amplitude above a gas flow of 18 sccm was ~1.8 times larger than that at 5 sccm, while the signal amplitude remains at a constant value from 5 sccm to 40 sccm when a 5% CO/SF_6 gas mixture (the data is not shown in Fig. 5) was fed in the DPAC. A same experimental phenomenon was observed for NO_2 detection with a 3.5 W blue diode laser [29]. These experimental results confirmed that an increase of the gas flow further enhances the detection signal amplitude in the case of a high optical excitation power. In a following experiment, a gas flow of 80 sccm was selected to avoid saturated and intermediate zones and generating a low noise based on Fig. 2(b).

With such a gas flow rate, an experiment was carried out to check the saturation level. A certified 500 ppm CO/SF_6 gas mixture was used. An experimental current modulation depth of 20 mA was chosen to obtain the optimal signal amplitudes. In order to measure the laser output power, a thermopile laser power meter was placed behind the DPAC instead of the beam dump mentioned above. As shown in Fig. 6, the calculated signal-to-noise ratios (SNRs) were plotted as a function of the actual output optical powers range from 30 mW to 9.5 W. The noise levels were defined as the standard deviations (1σ) of the output signal amplitudes with different powers in a pure SF_6 buffer gas. A linear fitting routine was implemented to verify the relationship between the optical power and the SNR. The calculated *R*-Square of 0.9998 confirms that our sensor system was not operated in saturation. Further evaluation tests were implemented with an actual mean power of 9.5 W to obtain an improved minimum detection limit.

5. Sensor performance optimization and assessment

For the PAS technique, the gas pressure is a critical parameter, since the laser wavelength modulation depth, *Q*-factor of the cell, absorption cross section of the absorbing molecular σ, and the total concentration (number density) *N* of the absorbing molecules are pressure dependent [30]. These pressure fluctuations may influence the precision of the sensor system significantly. In order to obtain optimal sensor performance, the gas pressure and modulation depth should be chosen appropriately. Fig. 7 shows the relationship between the SNR and the gas pressure from 230 Torr to 700 Torr. The concentration of the CO/SF_6 gas mixture was 500 ppm. The wavelength modulation depth was experimentally optimized at each gas pressure. A linear increase of the signal amplitude (*R*-Square ~ 0.998) was observed with increasing gas pressure. We selected atmospheric pressure as the operating pressure in order to avoid a pressure controller.

Different concentrations of a CO/SF_6 gas mixture range from 25 ppm to 500 ppm generated with a gas dilution system were fed into the DPAC. A 1-s time constant was set for the lock-in amplifier. As shown in Fig. 8, the mean signal amplitudes were recorded at different concentration levels. The observed result confirmed the linear response of this sensor system to the CO concentration in a SF_6 buffer gas. For a 50 ppm CO/SF_6 gas mixture, the SNR of 465 can be calculated from the ratio of the signal amplitude of 512 μV and the noise level of 1.1 μV. Thus, a minimum detection limit (1σ) of 110 ppb was obtained with a 9.5 W optical excitation power, which corresponds to a normalized noise equivalent absorption (NNEA) coefficient of 5.5×10^{-9} cm^{-1} W/$Hz^{1/2}$ with respect to the detection bandwidth and optical power.

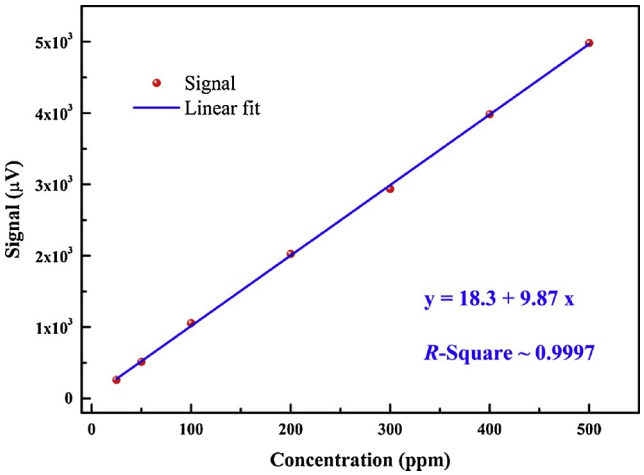

Fig. 8. Response linearity of the PAS-based CO sensor system for the SF_6 decomposition analysis.

6. Conclusions

In this work, a robust, compact and ppb level PAS-based CO sensor system for SF_6 decomposition detection was developed and demonstrated. Between the three CO absorption bands, its second overtone band is the weakest, which means the worst detection sensitivity. However, the second overtone band located in the NIR spectral region is interference-free from SF_6. In fact, the interference from SF_6 becomes stronger when the wavelength moves from the NIR to the MIR spectral region. We employed a two-stage fiber amplifier to amplify the optical excitation power from 10 mW to 10 W, which effectively compensates the weak absorption line strength. Moreover, we established a

theoretical model to describe and investigate the dynamic equilibrium processes of CO molecular activation and deactivation in the presence of the gas flow, which was verified experimentally. The results showed that the signal amplitude can be further enhanced by increasing the gas flow in the condition of high optical excitation power. With optimum design of the photoacoustic cell and optimal gas flow, a ppb-level detection sensitivity was achieved, which is comparable with that obtained with a MIR CO sensor. The reported CO sensor system will be deployed in an electric power system, together with our recently developed SO_2 and H_2S sensor systems [18,19] to further evaluate its performance in field applications.

Acknowledgements

Lei Dong acknowledges support by National Key R&D Program of China (2017YFA0304203), National Natural Science Foundation of China (NSFC) (61622503, 61575113, 61805132, 11434007), Changjiang Scholars and Innovative Research Team in University of Ministry of Education of China (IRT_17R70), 111 project (D18001), Outstanding Innovative Teams of Higher Learning Institutions of Shanxi, Foundation for Selected Young Scientists Studying Abroad, Sanjin Scholar (2017QNSJXZ-04) and Shanxi "1331KSC". Frank K. Tittel acknowledges support by the US National Science Foundation (NSF) ERC MIRTHE award and the Robert Welch Foundation (Grant #C0586). Xukun Yin acknowledges the financial support from the program of China Scholarships Council (No. 201808140194).

References

[1] R. Kurte, C. Beyer, H.M. Heise, D. Klockow, Application of infrared spectroscopy to monitoring gas insulated high-voltage equipment: electrode material-dependent SF_6 decomposition, Anal. Bioanal. Chem. 373 (2002) 639–646.
[2] E. Duffour, Molecular dynamic simulations of the collision between copper ions, SF_6 molecules and a polyethylene surface: a study of decomposition products and an evaluation of the self-diffusion coefficients, Macromol. Theory Simul. 19 (2010) 88–99.
[3] V. Spagnolo, P. Patimisco, S. Borri, G. Scamarcio, B.E. Bernacki, J. Kriesel, Part-per-trillion level detection of SF_6 using a single-mode fiber-coupled quantum cascade laser and a quartz enhanced photoacoustic sensor, Opt. Lett. 37 (2012) 4461–4463.
[4] J. Olthoff, R. Van Brunt, J. Herron, I. Sauers, Detection of trace disulfur decafluoride in sulfur hexafluoride by gas chromatography/mass spectrometry, Anal. Chem. 63 (1991) 726–732.
[5] S. Peng, G. Wu, W. Song, Q. Wang, Application of flower-like Zno nanorods gas sensor detecting SF_6 decomposition products, J. Nanomater. (2013) (2013) 875.
[6] X. Zhang, B. Yang, X. Wang, C. Luo, Effect of plasma treatment on multi-walled carbon nanotubes for the detection of H_2S and SO_2, Sensors (Basel) 12 (2012) 9375–9385.
[7] R. Cui, L. Dong, H. Wu, S. Li, L. Zhang, W. Ma, W. Yin, L. Xiao, S. Jia, F. Tittel, Highly sensitive and selective CO sensor using a 2.33 μm diode laser and wavelength modulation spectroscopy, Opt. Express 26 (2018) 24318–24328.
[8] A. Derdouri, J. Casanovas, R. Hergli, R. Grob, J. Mathieu, Study of the decomposition of wet SF_6, subjected to 50-Hz ac corona discharges, J. Appl. Phys. 65 (1989) 1852–1857.
[9] M.W. Sigrist, Mid-infrared laser-spectroscopic sensing of chemical species, J. Adv. Res. 6 (2015) 529–533.
[10] L. Dong, C. Li, N. Sanchez, A. Gluszek, R. Griffin, F. Tittel, Compact CH_4 sensor system based on a continuous-wave, low power consumption, room temperature interband cascade laser, Appl. Phys. Lett. 108 (2016) 011106.
[11] W. Ren, W. Jiang, F.K. Tittel, Single-QCL-based absorption sensor for simultaneous trace-gas detection of CH_4 and N_2O, Appl. Phys. B 117 (2014) 245–251.
[12] Y. Cao, N.P. Sanchez, W. Jiang, R.J. Griffin, F. Xie, L.C. Hughes, C. Zah, F.K. Tittel, Simultaneous atmospheric nitrous oxide, methane and water vapor detection with a single continuous wave quantum cascade laser, Opt. Express 23 (2015) 2121–2132.
[13] X. Yin, L. Dong, H. Zheng, X. Liu, H. Wu, Y. Yang, W. Ma, L. Zhang, W. Yin, L. Xiao, S. Jia, Impact of humidity on quartz-enhanced photoacoustic spectroscopy based CO detection using a NIR telecommunication diode laser, Sensors 16 (2016) 162.
[14] M. Mordmüller, M. Köhring, W. Schade, U. Willer, An electrically and optically cooperated QEPAS device for highly integrated gas sensors, Appl. Phys. B 119 (2015) 111–118.
[15] X. Zhang, H. Liu, J. Ren, J. Li, X. Li, Fourier transform infrared spectroscopy quantitative analysis of SF_6 partial discharge decomposition components, Spectrochim. Acta A. Mol. Biomol. Spectrosc. 136 (2015) 884–889.
[16] J. Luo, Y.H. Fang, Y.D. Zhao, A.J. Wang, D.C. Li, Y.Y. Li, Y. Liu, F.X. Cui, J. Wu, J.X. Liu, Research on the detection of SF_6 decomposition products based on non-resonant photoacoustic spectroscopy, Anal. Methods 7 (2015) 1200–1207.
[17] X. Zhang, Z. Cheng, X. Li, Cantilever enhanced photoacoustic spectrometry: quantitative analysis of the trace H_2S produced by SF_6 decomposition, Infrared Phys. Technol. 78 (2016) 31–39.
[18] X. Yin, L. Dong, H. Wu, W. Ma, L. Zhang, W. Yin, L. Xiao, S. Jia, F. Tittel, Ppb-level H_2S detection for SF_6 decomposition based on a fiber-amplified telecommunication diode laser and a background-gas-induced high-Q photoacoustic cell, Appl. Phys. Lett. 111 (2017) 031109.
[19] X. Yin, L. Dong, H. Wu, H. Zheng, W. Ma, L. Zhang, W. Yin, L. Xiao, S. Jia, F. Tittel, Highly sensitive SO_2 photoacoustic sensor for SF_6 decomposition detection using a compact mW-level diode-pumped solid-state laser emitting at 303 nm, Opt. Express 25 (2017) 32581–32590.
[20] A. Kosterev, F. Tittel, R. Koehler, C. Gmachl, F. Capasso, D.L. Sivco, A. Cho, S. Wehe, M. Allen, Thermoelectrically cooled quantum-cascade-laser-based sensor for the continuous monitoring of ambient atmospheric carbon monoxide, Appl. Opt. 41 (2002) 1169–1173.
[21] L. Dong, R. Lewicki, K. Liu, P.R. Buerki, M.J. Weida, F.K. Tittel, Ultra- sensitive carbon monoxide detection by using EC-QCL based quartz-enhanced photoacoustic spectroscopy, Appl. Phys. B 107 (2012) 275–283.
[22] Y. Ma, R. Lewicki, M. Razeghi, F. Tittel, QEPAS based ppb-level detection of CO and N_2O using a high power CW DFB-QCL, Opt. Express 21 (2013) 1008–1019.
[23] Y. He, Y. Ma, Y. Tong, X. Yu, F. Tittel, HCN ppt-level detection based on a QEPAS sensor with amplified laser and a miniaturized 3D-printed photoacoustic detection channel, Opt. Express 26 (2018) 9666–9675.
[24] H.P. Wu, L. Dong, H.D. Zheng, X.L. Liu, X.K. Yin, W.G. Ma, L. Zhang, W.B. Yin, S.T. Jia, F.K. Tittel, Enhanced near-infrared QEPAS sensor for sub-ppm level H_2S detection by means of a fiber amplified 1582 nm DFB laser, Sens. Actuators B-Chem. 221 (2015) 666–672.
[25] Z. Zhang, T. Pang, Y. Yang, H. Xia, X. Cui, P. Sun, B. Wu, Y. Wang, M. Sigrist, F. Dong, Development of a tunable diode laser absorption sensor for online monitoring of industrial gas total emissions based on optical scintillation cross-correlation technique, Opt. Express 24 (2016) A943–A955.
[26] H.P. Wu, A. Sampaolo, L. Dong, P. Patimisco, X.L. Liu, H.D. Zheng, X.K. Yin, W.G. Ma, L. Zhang, W.B. Yin, V. Spagnolo, S.T. Jia, F.K. Tittel, Quartz enhanced photoacoustic H_2S gas sensor based on a fiber-amplifier source and a custom tuning fork with large prong spacing, Appl. Phys. Lett. 107 (2015) 111104.
[27] The HITRAN database http://www.hitran.com.
[28] L. Rothman, I. Gordon, A. Barbe, et al., The HITRAN 2008 molecular spectroscopic database, J. Quant. Spectroscopy Rad. Transf. 110 (2009) 533–572.
[29] X. Yin, L. Dong, H. Wu, H. Zheng, W. Ma, L. Zhang, W. Yin, S. Jia, F. Tittel, Sub-ppb nitrogen dioxide detection with a large linear dynamic range by use of a differential photoacoustic cell and a 3.5 W blue multimode diode laser, Sens. Actuators B Chem. 247 (2017) 329–335.
[30] A. Miklos, P. Hess, Z. Bozoki, Application of acoustic resonators in photoacoustic trace gas analysis and metrology, Rev. Sci. Instrum. 72 (2001) 1937–1955.
[31] A. Miklós, Acoustic aspects of photoacoustic signal generation and detection in gases, Int. J. Thermophys. 36 (2015) 2285–2317.
[32] C.Y. Yuan, Z.X. Yan, G. Meng, Z.H. Li, L.P. Shang, Photoacoustic signal saturation characteristics of concentrated gases, Acta Phys. Sin. 59 (2010) 6908–6913.
[33] F.J.M. Harren, F.G.C. Bijnen, J. Reuss, L.A.C.J. Voesenek, C.W.P.M. Blom, Sensitive intracavity photoacoustic measurements with a CO_2 waveguide laser, Appl. Phys. B 50 (1990) 137–144.
[34] D.C. Dumitras, D.C. Dutu, C. Matei, A.M. Magureanu, M. Petrus, C. Popa, Laser photoacoustic spectroscopy: principles, instrumentation, and characterization, J. Optoelectron. Adv. Mater. 9 (2007) 3655–3701.